Inorganic Chemistry
Article
Cite This: Inorg. Chem. XXXX, XXX, XXX−XXX
pubs.acs.org/IC

The Influence of Cu and Al Additives on Reduction of Iron(III) Oxide: *In Situ* XRD and XANES Study

Olga A. Bulavchenko,[†,‡] Zakhar S. Vinokurov,[†,‡] Andrey A. Saraev,[†,‡] Anna M. Tsapina,[†] Alexander L. Trigub,[§] Evgeny Yu. Gerasimov,[†,‡] Alexey Yu. Gladky,[†] Alexander V. Fedorov,[†,‡] Vadim A. Yakovlev,[†,‡] and Vasily V. Kaichev*[,†,‡]

[†]Boreskov Institute of Catalysis, Ak. Lavrentiev Avenue, 5, Novosibirsk 630090, Russia
[‡]Novosibirsk State University, Pirogov Street, 2, Novosibirsk 630090, Russia
[§]National Research Center "Kurchatov Institute", Kurchatov Square 1, Moscow 123182, Russia

Supporting Information

ABSTRACT: The reduction of Fe-based nanocomposite catalysts doped with Al and Cu has been studied using *in situ* X-ray diffraction (XRD), *in situ* X-ray absorption near-edge structure (XANES), and temperature-programmed reduction (TPR) techniques. The catalysts have been synthesized by melting of iron, aluminum, and copper salts. According to XRD, the catalysts consist mainly of Fe_2O_3 and Al_2O_3 phases. Alumina is in an amorphous state, whereas iron oxide forms nanoparticles with the protohematite structure. The Al^{3+} cations are partially dissolved in the Fe_2O_3 lattice. Due to strong alumina−iron oxide interaction, the specific surface area of the catalysts increases significantly. TPR and XANES data indicate that copper forms highly dispersed surface CuO nanoparticles and partially dissolves in iron oxide. It has been shown that the reduction of iron(III) oxide by CO proceeds via two routes: a direct two-stage reduction of iron(III) oxide to metal ($Fe_2O_3 \rightarrow Fe_3O_4 \rightarrow Fe$) or an indirect three-stage reduction with the formation of FeO intermediate phases ($Fe_2O_3 \rightarrow Fe_3O_4 \rightarrow FeO \rightarrow Fe$). The introduction of Al into Fe_2O_3 leads to a decrease in the rate for all reduction steps. In addition, the introduction of Al stabilizes small Fe_3O_4 particles and prevents further sintering of the iron oxide. The mechanism of stabilization is associated with the formation of $Fe_{3-x}Al_xO_4$ solid solution. The addition of copper to the Fe−Al catalyst leads to the formation of highly dispersed CuO particles on the catalyst surface and a mixed oxide with a spinel-type crystalline structure similar to that of $CuFe_2O_4$. The low-temperature reduction of Cu^{2+} to Cu^0 accelerates the $Fe_2O_3 \rightarrow Fe_3O_4$ and $FeO \rightarrow Fe$ transformations but does not affect the $Fe_3O_4 \rightarrow FeO/Fe$ stages. These changes in the reduction properties significantly affect the catalytic performance of the Fe-based nanocomposite catalysts in the low-temperature oxidation of CO.

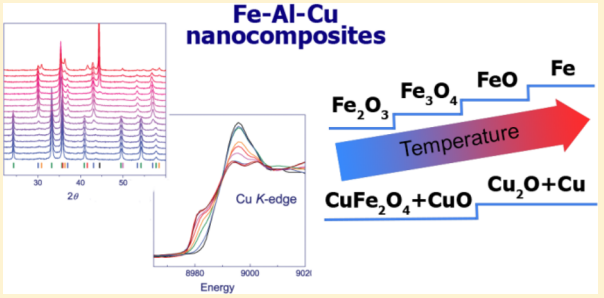

1. INTRODUCTION

Fe-based catalysts have been the subject of intense research in recent decades due to a wide application in various fields, such as water−gas shift (WGS) reactions,[1−5] the Fischer−Tropsch synthesis,[6] deep oxidation of CO and hydrocarbons,[7] partial oxidation of H_2S,[8] and ammonia synthesis.[1,9] The catalysts feature not only high activity in these reactions but also low cost and environmental safety. At the same time, the catalysts containing only supported iron oxides demonstrate insufficient activity and stability in the reactions mentioned above. As a result, many researchers are looking for ways to further improve the Fe-based catalysts. One of the ways for increasing catalytic activity, improving textural characteristics, and stabilizing the catalyst from sintering is using various promoters, such as Cu, Cr, and Al. Aluminum and chromium are used as textural promoters to prevent sintering and minimize surface area loss of the iron oxide phase.[10,11] Copper is usually applied to increase the catalytic activity.[5] Besides, the promoters can change the redox properties of the catalysts and thereby influence the catalytic performance.[12] Indeed, the reaction feeds in all above-mentioned catalytic processes contain reducing agents such as CO, H_2, or hydrocarbons (HC); thus, the phase composition and the chemical state of the Fe-based catalysts may be changed significantly under reaction conditions. This may lead to activation or deactivation of the catalysts. Moreover, some reactions may proceed via the redox mechanism when, for example, the catalyst is reduced by CO, H_2, or HC and then is oxidized by O_2 or H_2O. From this point of view, the investigation of the influence of different additives on the reduction of iron oxides is of great practical interest.

Usually, the reduction of pure iron(III) oxide involves several steps including the formation of the intermediate oxides such as magnetite (Fe_3O_4) and wustite (FeO).[13] The mechanism for the reduction of Fe_2O_3 by hydrogen varies

Received: December 6, 2018

DOI: 10.1021/acs.inorgchem.8b03403
Inorg. Chem. XXXX, XXX, XXX−XXX

with temperature, as reported by Pineau and co-workers.[14] The reduction of Fe_2O_3 to metallic iron proceeds via two-step $Fe_2O_3 \rightarrow Fe_3O_4 \rightarrow Fe$ or three-step $Fe_2O_3 \rightarrow Fe_3O_4 \rightarrow FeO \rightarrow Fe$ mechanisms depending on the temperature and H_2O/H_2 ratio and could be affected by the formation of metastable FeO intermediate phases.[13−15] The introduction of additives can lead to the formation of mixed oxides, the reduction mechanism of which is different from that for simple oxides. According to the literature studies, the addition of Cr,[16] Ce,[17] and Al[17] to hematite increases the transformation temperature of Fe_2O_3 to Fe_3O_4, whereas the addition of Ru, Os, Ag, Au,[18] and Cu[17] leads to a decrease in the reduction temperature. Zhao and co-workers[19] found that the doping with Ca increases the reduction rate of Fe_2O_3; especially Ca promotes the phase transition of FeO to metallic iron. Addition of Cu significantly decreases the reduction temperature of hematite to magnetite ($Fe_2O_3 \rightarrow Fe_3O_4$).[17]

It should be noted that the research on the reduction of catalysts was mostly carried out using temperature-programmed reduction by hydrogen (TPR-H_2), which does not show the real state of the catalyst, i.e., the phase composition and chemistry under reaction conditions. Certainly, this approach can be successfully used for studying pure iron oxides when the main routes of the reduction are predictable. However, the addition of dopants can lead to the formation of different types of solid solutions with iron oxide, the interaction of additives, the formation of new simple and mixed oxides, and metal nanoparticles at various stages of reduction, which can result in the acceleration or inhibition of the reduction reactions. In addition, there is a difference in the reduction by hydrogen or CO: the involvement of CO as a reducing agent may also produce iron carbide in an excessive CO environment. In order to obtain more detailed information about the reduction mechanism, another approach should be used: the approach based on the application of *in situ* techniques that are sensitive to both the chemical state of cations and the phase compositions. Earlier, such an approach based on a combined use of TPR-H_2, *in situ* X-ray diffraction, and X-ray photoelectron spectroscopy was applied for investigation of reduction of mixed Mn−Zr and Mn−Ga oxides.[20,21]

In this work, we use temperature-programmed reduction by CO (TPR-CO), XRD, and XANES spectroscopy to study *in situ* the behavior of CuO, Fe_2O_3, Al_2O_3−Fe_2O_3, and CuO−Al_2O_3−Fe_2O_3 nanocomposite catalysts during the reduction in CO. XRD provides information about the crystallographic structure and the phase composition, whereas XANES reveals the local structure and the oxidation state of cations. CuO−Al_2O_3−Fe_2O_3 has been chosen as the object of study because catalysts of such a type are actively used in the high-temperature WGS reaction and in the oxidation of CO.[10,22,23] To elucidate the role of the promoters (Cu and Al) in the reduction process, we investigated the reduction of the CuO−Al_2O_3−Fe_2O_3 nanocomposite catalysts by CO and compared the obtained results with the reduction of pure oxides (CuO and Fe_2O_3) and the Al_2O_3−Fe_2O_3 catalyst.

2. EXPERIMENTAL SECTION

The catalysts were prepared as follows: the salts of the precursors ($Fe(NO_3)_3{\cdot}9H_2O$, $Al(NO_3)_3{\cdot}9H_2O$, and $Cu(NO_3)_2{\cdot}3H_2O$) were mixed in the required ratios; then, the mixture was heated to give a homogeneous melt of salt hydrates and was kept at a temperature of 200 °C until water was completely removed; finally, the solid residue was calcined in air at 450 °C for 1 h and then at 700 °C for 1 h. Three nanocomposite catalysts with the following compositions were prepared—$Cu_{10}Fe_{74}Al_{16}$, $Cu_5Fe_{78}Al_{17}$, and $Fe_{82}Al_{18}$—where the indexes correspond to the CuO, Fe_2O_3, and Al_2O_3 content (wt %), respectively. Reference samples (α-Fe_2O_3 and CuO) were prepared in the same way. The samples were characterized by XRD, XANES, TPR-CO, the nitrogen adsorption technique, and transmission electron microscopy (TEM).

Temperature-programmed reduction was carried out in a 10% CO/He flow (20 sccm) using a ChemBET Pulsar TPR/TPD analyzer (QuantaChrome Instruments, USA). Before an experiment, each sample (about 70 mg) was dried in a He flow at 150 °C for 20 min. During the experiment, the sample was heated with a constant heating rate (20 °C/min) from the ambient temperature to 1000 °C. The CO consumption was measured with a thermal conductivity detector. To exclude the effect of evolving CO_2 on the detector reading, a NaOH trap was placed between the reactor and the detector. All TPR-CO profiles were normalized to the sample weight.

The phase composition was studied by XRD using a D8 Advance diffractometer (Bruker Corp., Germany) equipped with a Lynxeye linear detector. The diffraction patterns were obtained using the Ni-filtered Cu Kα radiation (λ = 1.5418 Å) in the $\theta/2\theta$ configuration. The phases were identified using the powder diffraction database PDF-4+. The crystallite size was estimated by the Scherrer formula.[24] The quantitative content of phases in the samples was found by the Rietveld method using the TOPAS program.

An *in situ* X-ray diffraction study was carried out in a flow of 1% CO in He using the same D8 Advance diffractometer equipped with a reactor chamber XRK-900 (Anton Paar GmbH, Austria). The total flow rate was 100 sccm. XRD patterns were collected stepwise in the temperature range from 30 to 700 °C with a step of 50 °C; the heating rate was 12 °C/min. The 2θ range from 21 to 60° was scanned using a step of 0.05°.

The XANES study was performed at the Structural Materials Science beamline at the Kurchatov Synchrotron Radiation Source (National Research Center "Kurchatov Institute", Moscow, Russia). The experimental station was described in detail elsewhere.[25] The spectra were obtained at the Cu K-edge in the transmission mode using a channel-cut Si(111) monochromator. Powder samples were pressed into thin self-supporting pellets, mounted to a stainless steel holder and then placed in a custom reaction chamber for *in situ* XANES measurements. To obtain an appropriate X-ray absorption, the samples were diluted with a fine powder of hexagonal BN. The reduction process was studied in a flow of 5% CO in N_2 at atmospheric pressure in the temperature range from the ambient temperature to 600 °C by the stepwise manner. Two custom-made gridded ionization chambers, filled with appropriate N_2−Ar mixtures, were used as detectors. The ionization currents were measured by Keithley 6487 digital picoamperemeters (Keithley Instruments LLC, USA). The energy scale was calibrated using the first inflection point of the Cu K-edge spectra at 8979 eV. The obtained data were analyzed using the ATHENA software.[26]

The specific surface area of the catalysts was determined by the Brunauer−Emmett−Teller (BET) method using nitrogen adsorption isotherms measured at the liquid nitrogen temperature with an automatic volumetric adsorption unit ASAP 2400 (Micromeritics Instrument Corp., USA).

TEM images were obtained using a JEM-2010 microscope (JEOL Ltd., Japan) at an accelerating voltage of 200 kV and a lattice resolution of 1.4 Å. Energy dispersive X-ray (EDX) analysis was carried out using an energy dispersive spectrometer with a Si XFlash detector (Bruker Corp., Germany) with an energy resolution of 128 eV.

3. RESULTS

3.1. As-Prepared Samples. Three as-prepared Fe-based nanocomposites and pure CuO and Fe_2O_3 have been studied by XRD, TEM, EDX, and the nitrogen adsorption technique. The main data are summarized in Table 1. The CuO sample is

DOI: 10.1021/acs.inorgchem.8b03403
Inorg. Chem. XXXX, XXX, XXX−XXX

Table 1. Characteristics of Catalysts: Phase Composition, Crystallite Size (CS), Elementary Cell Volume (V), and Specific Surface Area (S_{BET})

sample	phase composition	CS (Å)	V (Å^3)	S_{BET} (m^2/g)
CuO	CuO, JCPDS #48-1548	1000		0.4
Fe_2O_3	α-Fe_2O_3, JCPDS #33-664	>1500	301.8	6
$Fe_{82}Al_{18}$	α-Fe_2O_3, JCPDS #33-664	460	300.0	26
$Cu_5Fe_{78}Al_{17}$	α-Fe_2O_3, JCPDS #33-664	460	300.2	25
$Cu_{10}Fe_{74}Al_{16}$	α-Fe_2O_3, JCPDS #33-664 (80%)	480	300.8	29
	Fe_3O_4*, JCPDS #65-3107 (20%)	250		

a fine powder with monoclinic structure and a crystallite size of approximately 1000 Å. The Fe_2O_3 sample is identified as hematite (the rhombohedral structure) with a crystallite size above 1500 Å. Addition of Al into the iron oxide does not result in the appearance of aluminum-containing phases (e.g., Al_2O_3, $AlFeO_3$, or $AlFe_2O_3$); however, the lattice parameters of the hematite structure change, indicating the partial incorporation of aluminum cations into the Fe_2O_3 lattice. The $Cu_5Fe_{78}Al_{17}$ catalyst is also single-phase. Probably, the catalysts contain alumina and copper oxides, but Al_2O_3 and CuO could be in the form of extremely small crystallites which is out of the detection limit for XRD and/or they could be in an amorphous state. Indeed, Al_2O_3 in the amorphous state has been found in the catalysts by FTIR.[23] An increase in the copper content to 10 wt % ($Cu_{10}Fe_{74}Al_{16}$) leads to the formation of some oxide with a spinel structure Fe_3O_4*, probably containing Cu, Al, and Fe ions in its lattice. It should be noted that the addition of Al and Cu leads to a decrease in the crystallite size of Fe-containing oxides. The nanocomposites are characterized by a significantly higher specific surface area than CuO and Fe_2O_3 (Table 1).

According to TEM and EDX, the $Cu_5Fe_{78}Al_{17}$ nanocomposite consists of agglomerates with different morphology and chemistry (Figure 1a). The first type of agglomerates is represented by disordered hematite particles about 100−200 Å in size (Figure 1b). The phase is identified by observation of two interplanar distances of 2.7 and 3.6 Å that correspond to (104) and (012) hematite planes. EDX analysis indicates that these agglomerates are Fe-rich and contain 75, 19, and 6 atom % Fe, Al, and Cu, respectively (Figure 1c). This means that aluminum and a small amount of copper cations enter into the lattice of iron oxide. The agglomerates of the second type have the same shape as particles of alumina (Figure 1d). According to EDX, they are Al-rich and contain 12, 73, and 15 atom % Fe, Al, and Cu, respectively (Figure 1e). Hence, we can speculate that the Al-rich agglomerates contain alumina and small inclusions of hematite and that copper is mainly localized in the Al-rich agglomerates. Heating the Al-rich area by the electron beam for 1 min leads to the appearance of rounded particles of copper oxide with a particle size less than 1 nm (Figure S1).

In the sample $Cu_{10}Fe_{74}Al_{16}$, two different areas enriched with iron or aluminum are observed (Figure S2). The EDX analysis shows that these regions contain about 93, 6, 1 atom % and 3, 73, 24 atom % Fe, Al, and Cu, respectively. In addition, the observed Fe-rich particles have an interplanar distance of 2.92 Å, which corresponds to the (220) plane of the spinel structure (Figure S2b). These results agree well with the XRD data that exhibit the spinel phase (Table 1).

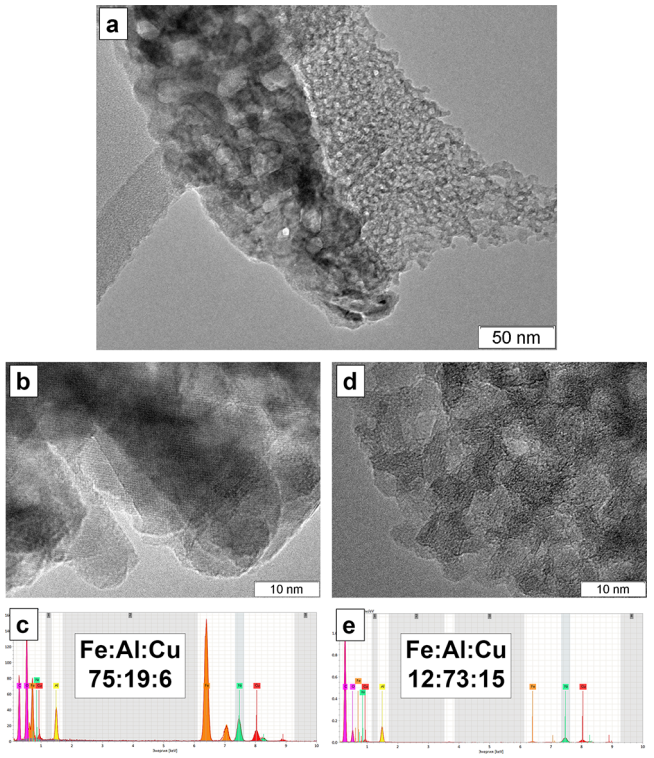

Figure 1. TEM images of $Cu_5Fe_{78}Al_{17}$ (a, b, d) and EDX spectra of Fe-rich (c) and Al-rich (e) regions.

TPR-CO was performed on all of the samples to examine their reducibility. The results are presented in Figure 2.

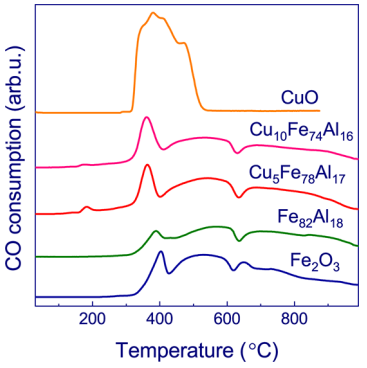

Figure 2. TPR-CO profiles of CuO, Fe_2O_3, and Fe-based nanocomposites.

Obviously, the TPR-CO profile of bulk CuO consists of a single peak between 310 and 540 °C, which is associated with the reduction of CuO to metallic copper. For undopped Fe_2O_3, there are three regions of CO consumption: a low-temperature sharp peak with a maximum at 405 °C and two broad high-temperature peaks located at 440−620 and 620−1000 °C, respectively. The first peak is assigned to the reduction of hematite (Fe_2O_3) to magnetite (Fe_3O_4); the second and third peaks with large CO consumption are attributed to the reduction of magnetite to FeO and FeO to Fe.[27−29] The TPR-CO profile of the $Fe_{82}Al_{18}$ catalyst has a similar shape. However, the low-temperature peak in this case is shifted to 390 °C. The addition of Cu leads to the appearance of a peak at 180 °C and to a shift of the following peak toward the lower temperatures. For example, the TPR-CO profile of the

DOI: 10.1021/acs.inorgchem.8b03403
Inorg. Chem. XXXX, XXX, XXX−XXX

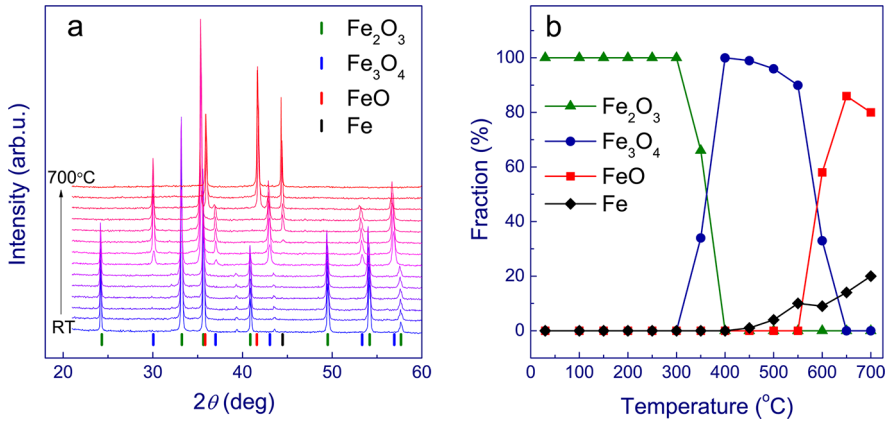

Figure 3. *In situ* XRD patterns of pure Fe_2O_3 collected during heating in a flow of 1% CO/He gas mixture (a) and quantitative phase composition as a function of the reduction temperature (b).

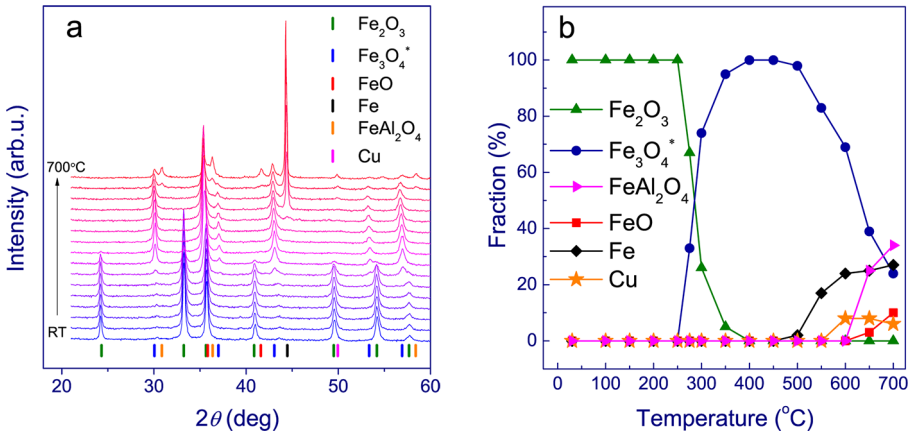

Figure 4. *In situ* XRD patterns of pure $Cu_5Fe_{78}Al_{17}$ collected during heating in a flow of 1% CO/He gas mixture (a) and quantitative phase composition as a function of the reduction temperature (b).

$Cu_5Fe_{78}Al_{17}$ catalyst contains two sharp low-temperature peaks at 180 and 360 °C. The first peak can be assigned to the reduction of highly dispersed CuO species over the catalyst surface.[30−32] The next peak at 360 °C is due to a complex process that includes simultaneous reduction of bulk Cu(II) and Fe(III) oxides. The maximum of this peak is even at a lower temperature than the reduction temperature of bulk CuO and Fe_2O_3. This means that the addition of Cu improves the reducibility of iron(III) oxide.

A similar synergetic effect was observed for Ni−Cu bimetallic catalysts in which the addition of Cu leads to a decrease in the reduction temperature of nickel oxide.[12] We can speculate that, in both cases, initially CuO is reduced to metallic copper, which facilitates the reduction of Fe_2O_3 or NiO. Because the highly dispersed CuO species exist on the catalyst surface, the reduction of hematite to magnetite starts at a temperature lower than the temperature of bulk CuO reduction. The TPR-CO profile of the $Cu_{10}Fe_{74}Al_{16}$ catalyst looks similar to that of $Cu_5Fe_{78}Al_{17}$. The first low-temperature peak decreases, indicating the enlargement of highly dispersed CuO species on the catalyst surface or Cu incorporation in the spinel phase (Table 1).

3.2. *In Situ* XRD Study. The phase transformations that occur during reduction of pure Fe_2O_3 and CuO oxides and the nanocomposites have been further studied by *in situ* XRD. In these experiments, the XRD patterns were collected during the stepwise heating of the samples in the 1% CO/He mixture from room temperature to 700 °C. The results of the investigation of Fe_2O_3 are presented in Figure 3. Hematite is the only crystalline phase detected at low temperatures. The observed peaks can be indexed in agreement with the expected rhombohedral (hexagonal) structure of α-Fe_2O_3 (space group $R\bar{3}c$). The peaks at the 2θ range of 24.20, 33.23, 35.68, 40.92, 49.54, 54.16, and 57.70° can be attributed to the 012, 104, 110, 113, 024, 116, and 018 reflections corresponding to pure α-Fe_2O_3. After heating to 350 °C, the diffraction peaks of Fe_2O_3 decrease and extra diffraction peaks appear at 30.11, 37.05, 43.03, 53.35, and 56.87° that correspond to Fe_3O_4 with a spinel structure (Figure 3a). At 400 °C, the diffraction peaks of Fe_2O_3 disappear, indicating that Fe_2O_3 completely reduces to Fe_3O_4 (space group $Fd3m$). Above 450 °C, the weak sharp peak at 44.53°, whose intensity increases slowly with temperature, can be attributed to metallic iron. The intense peaks at 36.00 and 41.80°, which correspond to FeO with the cubic structure (space group $Fm3m$), appear only at 600 °C, which is accompanied by the disappearance of the diffraction peaks of Fe_3O_4. The results of quantitative analysis are presented in Figure 3b. According to fraction weight estimation, which was performed by the Rietveld refinement, the Fe^0 content is small and does not exceed 20 wt %, whereas the FeO content achieves 80 wt %.

The reduction of Fe_2O_3 with hydrogen and CO has been the subject of much research.[14,15,29,33,34] Thermodynamic calculations show that the $Fe_2O_3 \rightarrow Fe_3O_4$ transformation occurs

DOI: 10.1021/acs.inorgchem.8b03403
Inorg. Chem. XXXX, XXX, XXX−XXX

easily in gas mixtures with a low reducing potential over a wide temperature range. The further reduction of Fe_3O_4 to metallic iron is a combination of two single-step reactions, Fe_3O_4 → FeO and FeO → Fe, that may proceed in parallel.[29] According to the XRD data, we observed first the direct transformation Fe_3O_4 → Fe and, at higher temperatures, the reduction Fe_3O_4 → FeO.

The results of the *in situ* XRD study of the reduction of $Cu_5Fe_{78}Al_{17}$ by CO are presented in Figure 4. Again, at low temperatures, the sample presents only the reflections characteristic of the rhombohedral hematite structure, without any other phases (Figure 4a). Heating from 30 to 600 °C leads to transformations similar to those seen in Figure 3 for the reduction of pure Fe_2O_3, but the presence of Cu and Al dopants changes the temperature of phase transitions (Figure 4b). The reduction of Fe_2O_3 to Fe_3O_4 begins at 275 °C, and 100% of Fe_2O_3 reduces at 400 °C. The further reduction of Fe_3O_4 is observed at 500 °C. It should be noted that the Fe_3O_4 reduction proceeds directly to metallic iron; however, Fe_3O_4 is not fully reduced even at 700 °C. Approximately 23 wt % of Fe_3O_4 remains in the catalyst. Only a small amount of FeO is detected at 650−700 °C. In addition, the diffraction peaks of $FeAl_2O_4$ are observed at 650−700 °C. According to our estimation, the $FeAl_2O_4$ content achieves 34 wt %. These findings indicate that the Fe_3O_4 phase contains not only Fe^{2+} and Fe^{3+} cations but also Al^{3+} cations. From this point of view, we designate this phase as Fe_3O_4*. Metallic copper (space group *Fm*3*m*) is also detected at 600−700 °C with a concentration of 5−8 wt % (discrepancies in the mass balance could be due to the presence of an X-ray amorphous phase).

Figure 5 summarizes the results of the *in situ* phase analysis and shows the temperature ranges for the existence of different

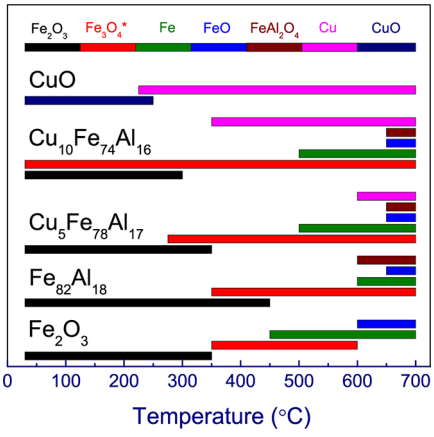

Figure 5. Phase composition of Fe_2O_3, $Fe_{82}Al_{18}$, $Cu_5Fe_{78}Al_{17}$, $Cu_{10}Fe_{74}Al_{16}$, and CuO in CO as a function of the reduction temperature.

phases in the reduction by CO for pure CuO, pure Fe_2O_3, and $Fe_{82}Al_{18}$, $Cu_5Fe_{78}Al_{17}$, and $Cu_{10}Fe_{74}Al_{16}$ nanocomposites. The XRD patterns of $Fe_{82}Al_{18}$ and $Cu_{10}Fe_{74}Al_{16}$ collected during heating in CO are shown in Figures S3 and S4. One can see that, first, pure Fe_2O_3 completely reduces to Fe_3O_4 and then Fe_3O_4 reduces to metallic iron and FeO. The introduction of aluminum (sample $Fe_{82}Al_{18}$) leads to the following changes: the temperature of Fe_2O_3 disappearance increases by 100 °C, the reaction products (FeO and metallic iron) appear at significantly higher temperatures compared with the pure iron oxide, and the intermediate phase of Fe_3O_4 is not completely reduced at 700 °C. In addition, a new $FeAl_2O_4$ phase appears at 600 °C.

In contrast, the addition of Cu destabilizes the hematite structure under reducing conditions. Indeed, for copper-containing catalysts ($Cu_5Fe_{78}Al_{17}$ and $Cu_{10}Fe_{74}Al_{16}$), the initial oxide with the hematite structure is reduced at the temperatures 100−150 °C lower than the reduction temperature of $Fe_{82}Al_{18}$ (Figure 5). The appearance of metallic iron in the copper-containing catalysts is also detected at lower temperatures than for $Fe_{82}Al_{18}$ but at higher temperatures than for pure Fe_2O_3. The metallic copper during the reduction of $Cu_5Fe_{78}Al_{17}$ and $Cu_{10}Fe_{74}Al_{16}$ appears at temperatures of 315 and 75 °C higher compared with pure CuO, respectively. Such a large difference in the reduction temperature of the $Cu_5Fe_{78}Al_{17}$ and $Cu_{10}Fe_{74}Al_{16}$ catalysts can be explained by the low sensitivity of XRD to copper in the highly dispersed state. The content of metallic copper does not increase with temperature (Figure 4b).

It should be stressed that prolonged reduction of the Fe_3O_4* intermediate phase is observed for aluminum containing catalysts. For $Fe_{82}Al_{18}$ and $Cu_5Fe_{78}Al_{17}$ nanocomposites, Fe_3O_4* is formed from hematite directly during the reduction, for the $Cu_{10}Fe_{74}Al_{16}$ nanocomposite, Fe_3O_4* exists in the initial state and its quantity increases during the reaction with CO. Figure 6 illustrates the changes in the lattice parameter of

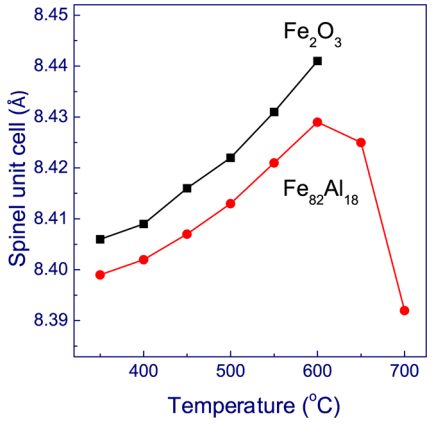

Figure 6. Unit cell parameter of spinel (Fe_3O_4*) for Fe_2O_3 and $Fe_{82}Al_{18}$ as a function of the reduction temperature.

Fe_3O_4* as a function of the temperature for $Fe_{82}Al_{18}$ in comparison with pure iron oxide. The parameter of pure Fe_3O_4 is higher than that of $Fe_{82}Al_{18}$ over the entire temperature range, which indicates the formation of a solid solution $Fe_{3-x}Al_xO_4$. The ionic radius of Al^{3+} (0.53 Å, CN = 6) is less than that of Fe^{3+} (0.65 Å, CN = 6).[35] Above 600 °C, the lattice parameter of $Fe_{3-x}Al_xO_4$ decreases, indicating a change in the composition of the solid solution (iron cations exit from the lattice). As a result, new phases of $FeAl_2O_4$, FeO, and metallic iron appear ($Fe_{3-x}Al_xO_4$ → $Fe_{3-y}Al_yO_4$ + $FeAl_2O_4$ + FeO + Fe, where $y > x$).

In situ XRD results show that the introduction of aluminum into Fe_2O_3 leads to (1) the slowdown of the reduction of Fe_2O_3 and Fe_3O_4, (2) the appearance of FeO and Fe at higher temperatures, (3) the formation of the intermediate $Fe_{3-x}Al_xO_4$ phase, and (4) the formation of aluminum-containing spinel-type $FeAl_2O_4$ and $Fe_{3-y}Al_yO_4$ phases as the reaction products.

DOI: 10.1021/acs.inorgchem.8b03403
Inorg. Chem. XXXX, XXX, XXX−XXX

The phase compositions of the Fe_2O_3, $Fe_{82}Al_{18}$, $Cu_5Fe_{78}Al_{17}$, $Cu_{10}Fe_{74}Al_{16}$, and CuO samples reduced in CO at 700 °C are given in Table 2. One can see that the addition of Cu into the

Table 2. Phase Composition Calculated from the XRD Data of Fe_2O_3, $Fe_{82}Al_{18}$, $Cu_5Fe_{78}Al_{17}$, $Cu_{10}Fe_{74}Al_{16}$, and CuO Samples Reduced at 700 °C

	phase composition (%)				
sample name	FeO	Fe	$FeAl_2O_4$	Fe_3O_4*	Cu
Fe_2O_3	80	20			
CuO					100
$Fe_{82}Al_{18}$	40	3	42	15	
$Cu_5Fe_{78}Al_{17}$	10	27	34	24	5
$Cu_{10}Fe_{74}Al_{16}$	8	30	29	24	9

Fe−Al system leads to an increase in the amount of metallic iron and to a significant decrease in the FeO content in the reaction products, whereas the total amount of the spinel-type oxides (Fe_3O_4* and $FeAl_2O_4$) changes slightly. Analysis of reaction products during reduction in CO and temperature intervals of phase transitions suggests that the introduction of Cu leads to the acceleration of the $Fe_2O_3 \rightarrow Fe_3O_4$ and FeO → Fe steps and has a weak effect on the reduction of Fe_3O_4* → FeO/Fe.

Probably, copper exists on the catalyst surface in the highly dispersed state. As a result, the sensitivity of XRD is not sufficient to identify the Cu-containing phases such as Cu and CuO nanoparticles, and the temperature of the formation of these phases obtained on the basis of *in situ* XRD data may be overestimated. To overcome this limit, we used XANES that can provide more correct information about the reduction process. X-ray absorption spectroscopy is a good alternative to XRD because this method allows one to study not only well-crystallized materials but also nanoparticles and amorphous materials.

3.3. *In Situ* XANES Analysis of $Cu_5Fe_{78}Al_{17}$ in the CO Flow. A series of *in situ* Cu K-edge XANES spectra acquired after exposing $Cu_5Fe_{78}Al_{17}$ to CO at different temperatures is presented in Figure 7a. The line shape of the Cu K-edge spectrum obtained at room temperature is typical of copper in the oxidized state. The spectrum contains a well-defined strong peak at 8995 eV that has been empirically assigned to the 1s → 4p electron dipole-allowed transition.[2,23,36] A quite similar spectrum is observed for $CuFe_2O_4$. The spectra of Cu_2O and CuO contain an extra pre-edge feature at 8981 and 8984 eV, respectively, that is almost absent in the spectrum of $CuFe_2O_4$. Metallic copper is characterized by a distinct pre-edge feature at 8981 eV and two almost equally intense peaks at 8994 and 9002 eV. The heating of the catalyst in CO leads to changing the line shape: the pre-edge feature intensity grows with temperature, indicating the changes in the local environment and chemical state of Cu. Substantial changes in the line shape of the Cu K-edge are seen in the temperature range between 150 and 400 °C.

The simplest approach in the XANES data processing is the linear combination fitting (LCF) method.[37,38] Having applied LCF, the spectrum is modeled by the least-squares fitting using a linear combination of known structures to fit an unknown spectrum. We performed linear combination fits of the obtained XANES spectra. The results are presented in Figure 7b. We have found that $Cu_5Fe_{78}Al_{17}$ consists mainly of $CuFe_2O_4$ and CuO. Approximately 80% of the copper cations

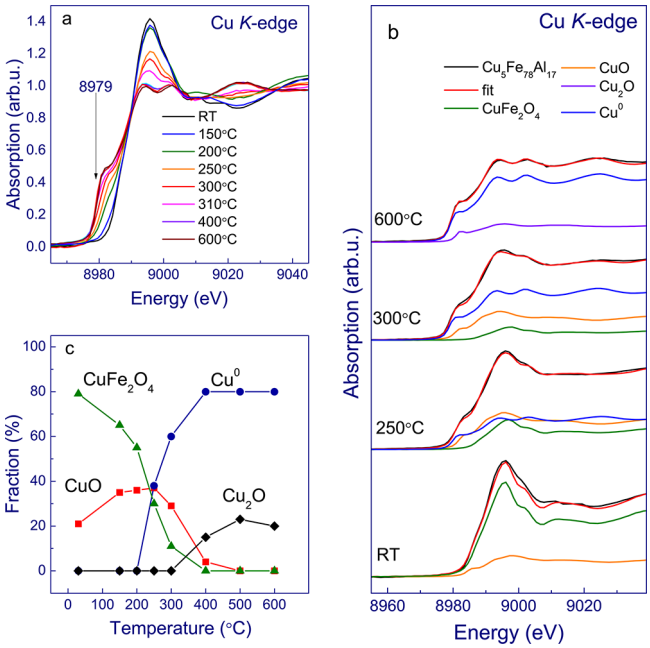

Figure 7. Normalized Cu K-edge XANES spectra of $Cu_5Fe_{78}Al_{17}$ obtained *in situ* in the 5% CO/He mixture at different temperatures (a). Linear combination fitting of the XANES spectra of $Cu_5Fe_{78}Al_{17}$ at room temperature and 250, 300, and 600 °C (b). The estimated concentration of individual components determined by the LCF analysis as a function of the reduction temperature (c).

exist in the $CuFe_2O_4$-like structure and 20% of the copper cations form CuO. The amount of the $CuFe_2O_4$-like phase decreases with temperature (Figure 7c). Simultaneously, we observe an increase in the amount of stable CuO up to 250 °C and appearance of Cu_2O and metallic Cu. The latter indicates the reduction of Cu^{2+} to Cu^{1+} and Cu^0.

The amount of metallic Cu achieves a maximum at 400 °C and then does not change; the Cu K-edge XANES spectrum of the reduced composite $Cu_5Fe_{78}Al_{17}$ catalyst is quite close to that of metallic copper. In contrast to the XRD data, we have detected metallic copper by XANES even at 250 °C. Taking into account the TPR-CO data (Figure 2), we can speculate that CuO directly reduces to metallic Cu near 250 °C to form copper clusters.[2] These copper clusters cannot be detected by XRD, but at higher temperatures, the clusters agglomerate to form nanoparticles. As a result, metallic Cu is observed only in $Cu_5Fe_{78}Al_{17}$ reduced at 600 °C (Figure 5). Cu_2O is not detected by XRD as well because it most likely is in an amorphous state. Moreover, the amount of copper in the Cu^{1+} state is small; however, it does not reduce to zero even at 600 °C. This means that Cu^{1+} cations incorporate into a structure of some mixed oxides where Cu atoms arrange in the fcc sublattice. Because XANES is sensitive to the local environment, the Cu K-edge spectra of these mixed oxides and Cu_2O may be very similar.

4. DISCUSSION

The above experimental results indicate that the introduction of a small amount of Al and Cu to iron(III) oxide changes its reducibility significantly. TPR-CO of Fe_2O_3 exhibits two regions of CO consumption (Figure 2). The low-temperature consumption of CO, observed as a sharp peak at 405 °C, is due to the fast reduction of Fe_2O_3 to Fe_3O_4. The second and third wide high-temperature peaks (between 440−620 and 620−

DOI: 10.1021/acs.inorgchem.8b03403
Inorg. Chem. XXXX, XXX, XXX−XXX

1000 °C) are associated with the $Fe_3O_4 \rightarrow FeO$ and $FeO \rightarrow Fe$ transformations. It should be noted that FeO is not completely reduced by CO even at 1000 °C.

We found that the crystallite size of Fe_2O_3 decreases from 1500 to 460 Å after doping by Al (Table 1). Simultaneously, the lattice parameter of Fe_2O_3 decreases slightly, which indicates the incorporation of aluminum into the Fe_2O_3 lattice.[23] According to TEM and EDX, aluminum exists in two different states: as amorphous Al_2O_3 and within the iron oxide structure (Figure 1). *In situ* XRD confirms the changes in the reduction temperature and reveals the formation of the intermediate Fe_3O_4* phase, which is more stable under reducing conditions. During the reduction of the $Al_2O_3-Fe_2O_3$ nanocomposite catalyst, $Fe_{3-y}Al_yO_4$, FeO, and metallic iron appear. $Fe_{3-y}Al_yO_4$ is not fully reduced in CO at 700 °C, whereas, during the reduction of pure Fe_2O_3, the intermediate Fe_3O_4 phase disappeared at 600 °C.

The introduction of 5% Cu into the Fe−Al catalyst leads to the formation of CuO and $CuFe_2O_4$, which are identified only by XANES spectroscopy. Most probably, CuO and $CuFe_2O_4$ exist in an amorphous state and/or form small clusters on the surface of hematite and alumina that cannot be detected by XRD. When the Cu concentration increases to 10%, XRD senses the appearance of a spinel structure such as Fe_3O_4*, which possibly includes both Al and Cu cations. The TPR results indicate that the reduction of Cu-doped catalysts starts at lower temperatures (Figure 2). A decrease in the reduction temperature is likely caused by the formation of highly dispersed CuO species.[30,32] In contrast to Al, Cu destabilizes hematite under reducing conditions.[39] Indeed, the main low-temperature peak of the CO consumption due to the $Fe_2O_3 \rightarrow Fe_3O_4$ transition shifts from 390 to 360 °C.

The possible explanation of these effects is governed by the different impacts of Al and Cu dopants on the reduction process. The addition of Al to iron(III) oxide leads to the suppression of the reduction steps, but the origin of influence varies. Aluminum is better dissolved in the spinel structure of Fe_3O_4 with the formation of a $Fe_{3-x}Al_xO_4$ solid solution rather than in Fe_2O_3 or FeO.[40] Therefore, the addition of Al inhibits the reduction of Fe_2O_3 mainly through a steric factor; the rate of $Fe_3O_4 \rightarrow FeO/Fe$ decreases due to the formation of mixed oxides. In contrast, the addition of Cu affects all of the reduction stages mostly via the formation of the metallic particles on the catalyst surface. According to the TPR and XANES data, Cu in the metallic state appears at 200−250 °C. It is suggested that metallic copper promotes the reduction of iron oxides through spillover. This means that the reductive agent (CO molecules) undergoes activation on the metallic clusters or nanoparticles and then migrates onto the iron oxide surface where the reduction process occurs. The improved reducibility of metal oxides was also observed for Cu−Ni and Cu−Mo−Ni oxide systems because of the formation of metallic copper.[12,41]

Because we consider the Fe-based nanocomposites as catalysts of the oxidation of CO, special attention must be paid to the formation of metallic species that are able to adsorb CO molecules and activate oxygen. *In situ* XRD indicates that the addition of Al hinders the reduction of iron(III) oxide to metallic iron, but the extra addition of Cu has the opposite effect. As a result, the lowest temperature of the formation of Fe nanoparticles is observed for the catalysts with a high Cu content: $Cu_{10}Fe_{74}Al_{16}$ (Figure 5). This catalyst also demonstrates the lowest temperature of the formation of Cu nanoparticles. Hence, we expect that the catalytic activity in the oxidation of CO should increase with the Cu content. In fact, another factor, namely, the enlargement of copper-containing particles with an increase in the copper content, should also be taken into account. As a result, the dependence of the activity of the $CuO-Al_2O_3-Fe_2O_3$ nanocomposite catalysts on copper concentration has a volcanic character.[23]

Another effect of reducibility on the catalytic performance dominates in the WGS reaction. The low-temperature WGS reaction proceeds at 350−500 °C,[42,43] and catalyst pretreatment involves the partial reduction of Fe_2O_3 to Fe_3O_4 using a gas mixture of H_2, CO, and CO_2 at 400 °C. In this case, it is important to avoid over-reduction of the magnetite active phase to lower carbides, oxides, or metallic iron. In industrial catalysts, chromium oxide serves as a textural promoter to inhibit sintering and stabilize the surface area of the magnetite phase. Many researchers believe that chromium can also enhance the high-temperature WGS activity by the formation of the $Cr^{3+} \leftrightarrow Cr^{6+}$ redox cycle.[44] However, the latest studies have shown that Cr additives do not function as a chemical promoter and only act as a structural stabilizer.[11] The mechanism of magnetite phase stabilization is related to the formation of $Fe_{3-x}Cr_xO_4$ solid solution.[5] A similar effect can be observed in the Al-doped catalysts.

Figure 8 demonstrates the crystal size of Fe_3O_4* for all of the catalysts as a function of the reduction temperature. For

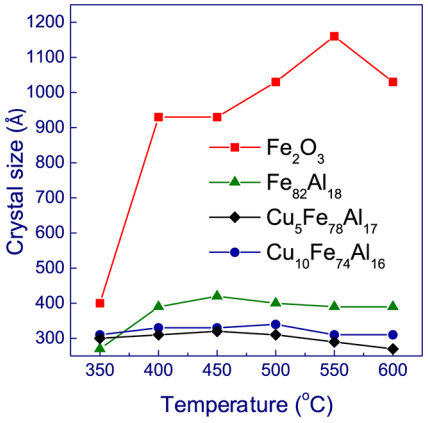

Figure 8. Crystal size of Fe_3O_4* as a function of reduction temperature.

the sample containing only iron oxide, the crystal size of Fe_3O_4* increases from 400 to 1100 Å, whereas, for $Fe_{82}Al_{18}$, it increases from 270 to 390 Å and changes insignificantly for Cu doped catalysts. Thus, the *in situ* XRD data demonstrate that the introduction of Al stabilizes the small Fe_3O_4 particles and prevents their further sintering. The mechanism of stabilization is related to the formation of $Fe_{3-x}Al_xO_4$ solid solution. By analogy with Cr, the introduction of aluminum prevents the over-reduction of iron oxide, due to the formation of a solid solution that is more stable under reducing conditions than Fe_3O_4. Unlike Cr and Al, the Cu promoter, however, functions as a chemical promoter by providing the formation of new highly active sites of metallic copper and Cu−Fe oxide interfacial sites.[5] It is well-known that Cu accelerates the oxide reduction due to the hydrogen spillover that could lead to over-reduction of iron oxide and have a negative effect in the high-temperature WGS reaction. Nevertheless, our study shows that, in spite of the formation of Cu nanoparticles

DOI: 10.1021/acs.inorgchem.8b03403
Inorg. Chem. XXXX, XXX, XXX−XXX

200−250 °C, the Fe_3O_4 content does not decrease up to 500 °C in CO.

5. CONCLUSIONS

The reduction of Fe_2O_3, CuO, and Al_2O_3−Fe_2O_3 and CuO−Al_2O_3−Fe_2O_3 nanocomposite catalysts was studied by TPR, *in situ* XRD, and *in situ* XANES techniques. We showed that in all of these cases the reduction of iron(III) oxide proceeds via the same two routes: a direct two-stage reduction of iron(III) oxide to metal ($Fe_2O_3 \rightarrow Fe_3O_4 \rightarrow Fe$) or an indirect three-stage reduction with the formation of FeO intermediate phases ($Fe_2O_3 \rightarrow Fe_3O_4 \rightarrow FeO \rightarrow Fe$). The addition of aluminum stabilizes hematite under reducing conditions, whereas the addition of Cu facilitates the reduction of hematite. The introduction of Al stabilizes small Fe_3O_4 particles and prevents further sintering of iron oxide; the mechanism of stabilization is associated with the formation of $Fe_{3-x}Al_xO_4$ solid solution. In the case of the Cu addition, the highly dispersed CuO particles over the hematite surface are formed. They can easily reduce to metal even at low temperature, which provides activation of CO. Both additives stabilize the catalytically active magnetite-like phase by the incorporation of Cu and Al cations into the Fe_3O_4 lattice. Another effect is the formation of alumina, which provides the high surface area of nanocomposites and again promotes the formation of highly dispersed CuO particles.

The approach used that is based on the combined application of TPR, *in situ* XRD, and *in situ* XANES is a very promising route to obtain detailed information about the state of catalyst under reducing conditions.

■ ASSOCIATED CONTENT

Supporting Information

The Supporting Information is available free of charge on the ACS Publications website at DOI: 10.1021/acs.inorgchem.8b03403.

TEM and EDX data, *in situ* XRD results, and quantitative phase composition (PDF)

■ AUTHOR INFORMATION

Corresponding Author

*E-mail: vvk@catalysis.ru.

ORCID

Olga A. Bulavchenko: 0000-0001-5944-2629
Zakhar S. Vinokurov: 0000-0002-2737-098X
Andrey A. Saraev: 0000-0001-9610-9921
Anna M. Tsapina: 0000-0002-2952-6669
Vasily V. Kaichev: 0000-0002-1516-2817

Author Contributions

The manuscript was written through contributions of all authors. All authors have given approval to the final version of the manuscript.

Notes

The authors declare no competing financial interest.

■ ACKNOWLEDGMENTS

This work was supported by Russian Science Foundation, Grant No. 17-73-20157.

■ REFERENCES

(1) Edwards, M. A.; Whittle, D. M.; Rhodes, C.; Ward, A. M.; Rohan, D.; Shannon, M. D.; Hutchings, G. J.; Kiely, C. J. Microstructural Studies of the Copper Promoted Iron Oxide/Chromia Water-Gas Shift Catalyst. *Phys. Chem. Chem. Phys.* **2002**, *4*, 3902−3908.

(2) Wang, X.; Hanson, J. C.; Frenkel, A. I.; Kim, J.-Y.; Rodriguez, J. A. Time-Resolved Studies for the Mechanism of Reduction of Copper Oxides with Carbon Monoxide: Complex Behavior of Lattice Oxygen and the Formation of Suboxides. *J. Phys. Chem. B* **2004**, *108*, 13667−13673.

(3) Estrella, M.; Barrio, L.; Zhou, G.; Wang, X.; Wang, Q.; Wen, W.; Hanson, J. C.; Frenkel, A. I.; Rodriguez, J. A. In Situ Characterization of $CuFe_2O_4$ and Cu/Fe_3O_4 Water−Gas Shift Catalysts. *J. Phys. Chem. C* **2009**, *113*, 14411−14417.

(4) Rodriguez, J. A.; Hanson, J. C.; Stacchiola, D.; Senanayake, S. D. In Situ/Operando Studies for the Production of Hydrogen Through the Water-Gas Shift on Metal Oxide Catalysts. *Phys. Chem. Chem. Phys.* **2013**, *15*, 12004−12025.

(5) Zhu, M.; Rocha, T. C. R.; Lunkenbein, T.; Knop-Gericke, A.; Schlögl, R.; Wachs, I. E. Promotion Mechanisms of Iron Oxide-Based High Temperature Water-Gas Shift Catalysts by Chromium and Copper. *ACS Catal.* **2016**, *6*, 4455−4464.

(6) Li, S.; Krishnamoorthy, S.; Li, A.; Meitzner, G. D.; Iglesia, E. Promoted Iron-Based Catalysts for the Fischer−Tropsch Synthesis: Design, Synthesis, Site Densities, and Catalytic Properties. *J. Catal.* **2002**, *206*, 202−217.

(7) Schoch, R.; Huang, H.; Schünemann, V.; Bauer, M. A New Iron-Based Carbon Monoxide Oxidation Catalyst: Structure−Activity Correlation. *ChemPhysChem* **2014**, *15*, 3768−3775.

(8) Bukhtiyarova, G. A.; Bukhtiyarov, V. I.; Sakaeva, N. S.; Kaichev, V. V.; Zolotovskii, B. P. XPS Study of the Silica-Supported Fe-Containing Catalysts for Deep or Partial H_2S Oxidation. *J. Mol. Catal. A: Chem.* **2000**, *158*, 251−255.

(9) Arabczyk, W.; Jasińska, I.; Lubkowski, K. The Surface Properties of Iron Catalyst for Ammonia Synthesis. *React. Kinet. Catal. Lett.* **2004**, *83*, 385−392.

(10) Zhang, L.; Wang, X.; Millet, J.-M. M.; Matter, P. H.; Ozkan, U. S. Investigation of Highly Active Fe-Al-Cu Catalysts for Water-Gas Shift Reaction. *Appl. Catal., A* **2008**, *351*, 1−8.

(11) Patlolla, A.; Carino, E. V.; Ehrlich, S. N.; Stavitski, E.; Frenkel, A. I. Application of Operando XAS, XRD, and Raman Spectroscopy for Phase Speciation in Water Gas Shift Reaction Catalysts. *ACS Catal.* **2012**, *2*, 2216−2223.

(12) Smirnov, A. A.; Khromova, S. A.; Bulavchenko, O. A.; Kaichev, V. V.; Saraev, A. A.; Reshetnikov, S. I.; Bykova, M. V.; Trusov, L. I.; Yakovlev, V. A. Effect of the Ni/Cu Ratio on the Composition and Catalytic Properties of Nickel-Copper Alloy in Anisole Hydrodeoxygenation. *Kinet. Catal.* **2014**, *55*, 69−78.

(13) Ramadan, W.; Zaki, M. I.; Fouad, N. E.; Mekhemer, G. A. H. Particle Characteristics and Reduction Behavior of Synthetic Magnetite. *J. Magn. Magn. Mater.* **2014**, *355*, 246−253.

(14) Pineau, A.; Kanari, N.; Gaballah, I. Kinetics of Reduction of Iron Oxides by H_2: Part II. Low Temperature Reduction of Magnetite. *Thermochim. Acta* **2007**, *456*, 75−88.

(15) Zieliński, J.; Zglinicka, I.; Znak, L.; Kaszkur, Z. Reduction of Fe_2O_3 with Hydrogen. *Appl. Catal., A* **2010**, *381*, 191−196.

(16) Reddy, G. K.; Gunasekara, K.; Boolchand, P.; Smirniotis, P. G. Cr- and Ce-Doped Ferrite Catalysts for the High Temperature Water−Gas Shift Reaction: TPR and Mossbauer Spectroscopic Study. *J. Phys. Chem. C* **2011**, *115*, 920−930.

(17) Meshkani, F.; Rezaei, M. Preparation of Nanocrystalline Metal (Cr, Al, Mn, Ce, Ni, Co and Cu) Modified Ferrite Catalysts for the High Temperature Water Gas Shift Reaction. *Renewable Energy* **2015**, *74*, 588−598.

(18) Venugopal, A.; Scurrell, M. S. Low Temperature Reductive Pretreatment of Au/Fe_2O_3 Catalysts, TPR/TPO Studies and Behaviour in the Water−Gas Shift Reaction. *Appl. Catal., A* **2004**, *258*, 241−249.

DOI: 10.1021/acs.inorgchem.8b03403
Inorg. Chem. XXXX, XXX, XXX−XXX

(19) Zhao, Z.-l.; Tang, H.-q.; Guo, Z.-c. Effects of CaO on Precipitation Morphology of Metallic Iron in Reduction of Iron Oxides Under CO Atmosphere. *J. Iron Steel Res. Int.* **2013**, *20*, 16−24.
(20) Bulavchenko, O. A.; Vinokurov, Z. S.; Afonasenko, T. N.; Tsyrul'nikov, P. G.; Tsybulya, S. V.; Saraev, A. A.; Kaichev, V. V. Reduction of Mixed Mn−Zr Oxides: in Situ XPS and XRD Studies. *Dalton Transactions* **2015**, *44*, 15499−15507.
(21) Bulavchenko, O. A.; Venediktova, O. S.; Afonasenko, T. N.; Tsyrul'nikov, P. G.; Saraev, A. A.; Kaichev, V. V.; Tsybulya, S. V. Nonstoichiometric Oxygen in Mn−Ga−O Spinels: Reduction Features of the Oxides and their Catalytic Activity. *RSC Adv.* **2018**, *8*, 11598−11607.
(22) Popa, T.; Xu, G.; Barton, T. F.; Argyle, M. D. High Temperature Water Gas Shift Catalysts with Alumina. *Appl. Catal., A* **2010**, *379*, 15−23.
(23) Fedorov, A. V.; Tsapina, A. M.; Bulavchenko, O. A.; Saraev, A. A.; Odegova, G. V.; Ermakov, D. Y.; Zubavichus, Y. V.; Yakovlev, V. A.; Kaichev, V. V. Structure and Chemistry of Cu−Fe−Al Nanocomposite Catalysts for CO Oxidation. *Catal. Lett.* **2018**, *148*, 3715−3722.
(24) Langford, J. I.; Wilson, A. J. C. Scherrer after Sixty Years: A Survey and Some New Results in the Determination of Crystallite Size. *J. Appl. Crystallogr.* **1978**, *11*, 102−113.
(25) Veligzhanin, A. A.; Zubavichus, Y. V.; Chernyshov, A. A.; Trigub, A. L.; Khlebnikov, A. S.; Nizovskii, A. I.; Khudorozhkov, A. K.; Beck, I. É.; Bukhtiyarov, V. I. An in Situ Sell for Investigation of the Catalyst Structure Using Synchrotron Radiation. *J. Struct. Chem.* **2010**, *51*, 20−27.
(26) Ravel, B.; Newville, M. ATHENA, ARTEMIS, HEPHAESTUS: Data Analysis for X-ray Absorption Spectroscopy Using IFEFFIT. *J. Synchrotron Radiat.* **2005**, *12*, 537−541.
(27) Cao, J.-L.; Wang, Y.; Yu, X.-L.; Wang, S.-R.; Wu, S.-H.; Yuan, Z.-Y. Mesoporous CuO−Fe_2O_3 Composite Catalysts for Low-Temperature Carbon Monoxide Oxidation. *Appl. Catal., B* **2008**, *79*, 26−34.
(28) Amini, E.; Rezaei, M.; Sadeghinia, M. Low Temperature CO Oxidation Over Mesoporous $CuFe_2O_4$ Nanopowders Synthesized by a Novel Sol-Gel Method. *Chin. J. Catal.* **2013**, *34*, 1762−1767.
(29) Chen, H. S.; Zheng, Z.; Chen, Z. W.; Bi, X. T. T. Reduction of Hematite (Fe_2O_3) to Metallic Iron (Fe) by CO in a Micro Fluidized Bed Reaction Analyzer: A Multistep Kinetics Study. *Powder Technol.* **2017**, *316*, 410−420.
(30) Luo, M.-F.; Fang, P.; He, M.; Xie, Y.-L. In Situ XRD, Raman, and TPR Studies of CuO/Al_2O_3 Catalysts for CO Oxidation. *J. Mol. Catal. A: Chem.* **2005**, *239*, 243−248.
(31) Águila, G.; Gracia, F.; Cortés, J.; Araya, P. Effect of Copper Species and the Presence of Reaction Products on the Activity of Methane Oxidation on Supported CuO Catalysts. *Appl. Catal., B* **2008**, *77*, 325−338.
(32) Svintsitskiy, D. A.; Kardash, T. Y.; Stonkus, O. A.; Slavinskaya, E. M.; Stadnichenko, A. I.; Koscheev, S. V.; Chupakhin, A. P.; Boronin, A. I. In Situ XRD, XPS, TEM, and TPR Study of Highly Active in CO Oxidation CuO Nanopowders. *J. Phys. Chem. C* **2013**, *117*, 14588−14599.
(33) Weiss, B.; Sturn, J.; Voglsam, S.; Winter, F.; Schenk, J. Industrial Fluidised Bed Direct Reduction Kinetics of Hematite Ore Fines in H_2 Rich Gases at Elevated Pressure. *Chem. Eng. Sci.* **2011**, *66*, 703−708.
(34) Sun, Y. S.; Han, Y. X.; Gao, P.; Li, G. F. Investigation of Kinetics of Coal Based Reduction of Oolitic Iron Ore. *Ironmaking Steelmaking* **2014**, *41*, 763−768.
(35) Shannon, R. D. Revised Effective Ionic Radii and Systematic Studies of Interatomic Distances in Halides and Chalcogenides. *Acta Crystallogr., Sect. A: Cryst. Phys., Diffr., Theor. Gen. Crystallogr.* **1976**, *32*, 751−767.
(36) Kau, L. S.; Spira-Solomon, D. J.; Penner-Hahn, J. E.; Hodgson, K. O.; Solomon, E. I. X-ray Absorption Edge Determination of the Oxidation State and Coordination Number of Copper. Application to the Type 3 Tite in Rhus Vernicifera Laccase and its Reaction with Oxygen. *J. Am. Chem. Soc.* **1987**, *109*, 6433−6442.
(37) Hsiao, M. C.; Wang, H. P.; Yang, Y. W. EXAFS and XANES Studies of Copper in a Solidified Fly Ash. *Environ. Sci. Technol.* **2001**, *35*, 2532−2535.
(38) Gaur, A.; Shrivastava, B. D.; Joshi, S. K. Copper K-edge XANES of Cu(I) and Cu(II) Oxide Mixtures. *J. Phys. Conf. Ser.* **2009**, *190*, No. 012084.
(39) Yuzbasi, N. S.; Abdala, P. M.; Imtiaz, Q.; Kim, S. M.; Kierzkowska, A. M.; Armutlulu, A.; van Beek, W.; Muller, C. R. The Effect of Copper on the Redox Behaviour of Iron Oxide for Chemical-Looping Hydrogen Production Probed by in Situ X-ray Absorption Spectroscopy. *Phys. Chem. Chem. Phys.* **2018**, *20*, 12736−12745.
(40) Raghavan, V. Al-Fe-O (Aluminum-Iron-Oxygen). *J. Phase Equilib. Diffus.* **2010**, *31*, 367−367.
(41) Kukushkin, R. G.; Bulavchenko, O. A.; Kaichev, V. V.; Yakovlev, V. A. Influence of Mo on Catalytic Activity of Ni-Based Catalysts in Hydrodeoxygenation of Esters. *Appl. Catal., B* **2015**, *163*, 531−538.
(42) Rhodes, C.; Hutchings, G. J.; Ward, A. M. Water-Gas Shift Reaction: Finding the Mechanistic Boundary. *Catal. Today* **1995**, *23*, 43−58.
(43) Reddy, G. K.; Gunasekera, K.; Boolchand, P.; Dong, J.; Smirniotis, P. G. High Temperature Water Gas Shift Reaction over Nanocrystalline Copper Codoped-Modified Ferrites. *J. Phys. Chem. C* **2011**, *115*, 7586−7595.
(44) Lee, D.-W.; Lee, M. S.; Lee, J. Y.; Kim, S.; Eom, H.-J.; Moon, D. J.; Lee, K.-Y. The Review of Cr-Free Fe-Based Catalysts for High-Temperature Water-Gas Shift Reactions. *Catal. Today* **2013**, *210*, 2−9.

DOI: 10.1021/acs.inorgchem.8b03403
Inorg. Chem. XXXX, XXX, XXX−XXX